Statics of Pin Corona Charger in Electrophotography*

Hiroyuki Kawamoto✦

Department of Mechanical Engineering, Waseda University, Shinjyuku, Tokyo, Japan

Statics of a pin electrode in a pin-to-plate system has been investigated to utilize the system for the new low ozone charger and to clarify the fundamental mechanism of bead carry-out in the two-component magnetic brush development subsystem of electrophotography. The electrostatic force in the system was measured and numerically calculated with a static unipolar model. Calculated voltage-current characteristics qualitatively agreed with those measured. Electrostatic force was also measured and calculated. Although extremely small electrostatic pull force was induced if discharge did not take place, the force became repulsive and relatively large when the corona discharge took place. Force in negative corona was almost the same as in positive corona. Calculated force without discharge agreed with the measured but the calculation did not simulate repulsive characteristics at corona discharging. Convection of air must be included in the model.

Journal of Imaging Science and Technology 45: 556–564 (2001)

Introduction

One of the most important issues of electrophotography technology is to reduce ozone emitted by charging and transferring devices, because not only does ozone damage photoreceptors and consequently causes deterioration of images, but it is also harmful for humans.[1] Although the corona chargers,[2] corotrons and scorotrons, have been most widely used in spite of large ozone emission,[3] a new charging device, a biased contact charger roller, has been developed in the late of 1980's to realize extremely low ozone emission.[4,5] The system consists of a highly electroresistive elastomer roller and a power supply. DC voltage superposed on AC voltage is applied between the photoreceptor drum and the charger roller. The electrical micro-discharge in the vicinity of the nip controls the charging of the photoreceptor.[6] Although ozone is formed in this system, it is extremely small.[7] An ozone filter is usually not necessary to satisfy an environmental standard. However, the contact charger roller is used only in low-speed machines, because the photoreceptor rapidly wears in this system due to the mechanical contact between the charger roller and the photoreceptor. Alternative discharge current induced by the application of AC voltage accelerates wear of the photoreceptor, because active ions generated in the vicinity of the contact area attack the organic photoconductor. It is believed that the wear mechanism is similar to ion etching. Furthermore, it is difficult to realize uniform charging using this charger for high-speed machines.

Another new low ozone charger was proposed by Furukawa and co-workers.[8,9] It has pin (saw-tooth) electrodes to which DC high voltage is applied through each resistor as schematically shown in Fig. 1. It was confirmed that interposed resistors control fluctuation and dispersion of discharge current from each discharge electrode. Consequently it uniformly charges the photoreceptor with less discharge current and an amount of generated ozone is less than that of the former charging device with parallel-connected saw-tooth electrodes to which high voltage is directly applied. Kawamoto[10] has established a theoretical model to calculate ozone emission from this new device applicable for high-speed machines. Results of the calculation were compared with experimental results and some fundamental characteristics and feasibility for the electrophotography charger were discussed. It was cited that the pin charger has a potential to realize extremely low ozone emission. However, several subjects to be overcome still exist to put the charger to practical use.

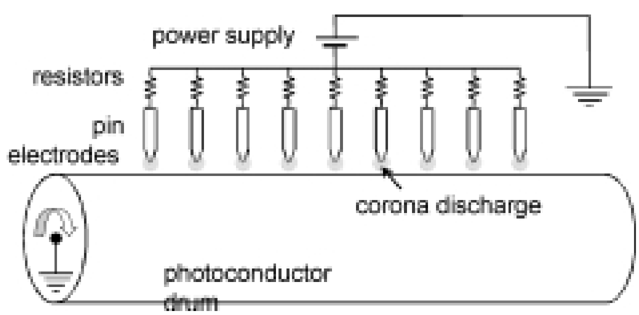

Figure 1. Schematic drawing of corona charger with parallel-connected pin electrodes to which high voltage is applied through each resistor.

Original manuscript received July 11, 2001

✦ IS&T Fellow

kawa@mn.waseda.ac.jp

*Previously presented at IS&T's NIP16: International Conference on Digital Printing Technologies, October 15-20, 2000, Vancouver, B.C. Canada.

Statics and dynamics of the discharge electrode are the other issues of this charger for realizing uniform charging, especially in the case where the stiffness of the discharge electrode is low. This is the case when a brush or magnetic bead chains are used as the pin electrodes. The electrode is deformed and/or abnormal vibration is induced by the electrostatic force. A series of investigation has been conducted on the kinetics of a wire-to-plate discharge system to clarify the mechanism of lateral oscillation that is sometimes observed in the corona charger used for a polyester film manufacturing machine.[11] It was reported that in the worst case, the vibration caused breakdown of the wire and then an effective countermeasure was proposed. On the other hand, no systematic study has been performed for kinetics of the pin-to-plate system except for the measurement of corona-induced force per hanging water drop from a high voltage transmission line and ionic wind in the mechanism of corona induced vibration.[12]

In this study, at the first phase of the kinetic investigation, the author has studied the electrostatic force acting on the pin electrode in a pin-to-plate corona discharge system. The present investigation is expected to be utilized for the design of the new low ozone charger in electrophotography, for example, determination of the stiffness of the pin electrode. In the mean time, a conductive magnetic brush development subsystem[2] in electrophotography is assumed a comprising a pin-to-plate system; a bead chain corresponds to the pin and photoconductor is the plate electrode. If carrier beads escape from the developer sleeve and adhere to the photoconductor surface, they cause serious image defects. Although many kinds of forces, such as magnetic, centrifugal, and van der Waals, are related to the separation of carrier beads from the chain, the electrostatic force is one of the major factors. The present work is also utilized for the clarification of this phenomenon called “bead carry-out.”[2]

Modeling

Because the electric conduction in a field of gas discharge is determined not only by the electrostatic potential ϕ but also by the charge density ρ, two coupled partial differential equations govern the static unipolar field.[13,14]

$$\nabla \cdot \left(-\omega\rho\nabla\phi\right) = 0 \quad \text{(continuity equation of charge)}, \quad (1)$$

$$-\varepsilon_0\nabla^2\phi = \rho \quad \text{(Poisson's equation)}, \quad (2)$$

where ω is the mobility of charged particles and ε_0 is the permittivity of free space. Diffusion and convection of charged particles are neglected. Boundary conditions with respect to the potential are simply derived from the fact that the potential difference between the gas discharge electrode and the collecting electrode is equal to the applied voltage V_0.

$$\phi = V_0 \quad \text{at discharge electrode}, \quad (3\text{-}1)$$

$$\phi = 0 \quad \text{at collecting electrode}. \quad (3\text{-}2)$$

On the other hand, because the boundary condition for the charge density is not known, it is assumed in this model that the electric field E at the surface of the discharging electrode is kept at a constant value E_0, which is equal to the calculated electrostatic field strength determined by the measured corona onset voltage in a coaxial electrode configuration. The adequacy of this assumption has been confirmed in the coaxial cylindrical corona discharge system.[14]

$$E = -\boldsymbol{n}\cdot\nabla\phi \le E_0 \ (= 14.55 \times 10^6 \text{ V/m}) \quad \text{at discharge electrode}, \quad (4)$$

where $\boldsymbol{n}$ is the unit normal vector to the boundary.

Integration of the current density $\omega\rho E$ over the whole surface of the electrode S yields the total discharge current I.

$$I = \int \omega\rho E \, dS. \quad (5)$$

The electrostatic force F to the electrode is calculated based on the Maxwell’s stress tensor method.

$$F = \frac{1}{2}\varepsilon \int E^2 \, dS. \quad (6)$$

After the electrostatic potential ϕ and the charge density ρ are derived from two coupled partial differential in Eqs. 1 and 2, satisfying the boundary conditions of Eqs. 3 and 4, the total discharge current I and the electrostatic force F are determined by the integral in Eqs. 5 and 6 respectively, for the given geometry and the applied voltage.

Numerical Method

Figure 2 shows a flowchart of the numerical method. Detailed procedure is as follows:

i) The calculation starts with the low applied voltage, less than the corona onset voltage. Initial value of ρ is assumed to be uniform and extremely low ($\rho_{initial}$ = 10^{-10} C/m^3).

ii) Two differentials, Eqs. 1 and 2, are solved independently with respect to ϕ under the boundary condition in Eq. 3 for the differential Eq. 1 and the boundary conditions in Eqs. 3 and 4 for Eq. 2. Poisson’s Eq. 2 must satisfies the boundary conditions for both Eq. 3-1 and Eq. 4 simultaneously at the discharge electrode. The concrete calculation procedure is that, at the first place, the Eq. 2 is calculated under the fixed boundary condition in Eq. 3-1, and if the calculated electric field on the discharge electrode exceeds the threshold E_0, the boundary condition at the corresponding boundary is replaced by Eq. 4.

iii) Distributions of the electric field, E_1 and E_2, corresponding to two calculated potential distributions, ϕ_1 and ϕ_2, are calculated separately. The subscripts 1 and 2 indicate the continuity equation of charge in Eq. 1 and Poisson’s Eq. 2, respectively.

iv) The calculations ii) and iii) are repeated with the revised charge density distribution,

$$\rho_i = \rho_{i-1}\left(1 + 2K\,\frac{E_1 - E_2}{E_1 + E_2}\right),$$

until $2\,|\,\phi_1 - \phi_2\,|/(\phi_1 + \phi)_2 < 10^{-4}$, where K is a relaxation coefficient and the subscript i is an iteration step.

v) Total discharge current I and the electrostatic force F are calculated by a simple numerical integration method.

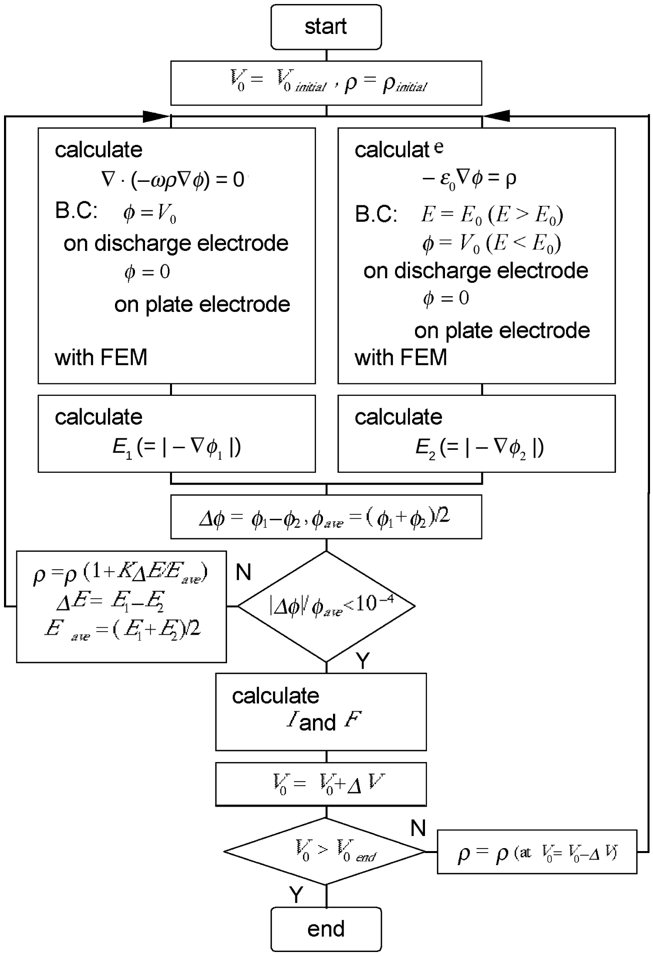

Figure 2. Flowchart of numerical method.

vi) The applied voltage is increased and the procedures ii) to v) are repeated until $V_0 = V_{0end}$. The charge density of the former voltage step is adapted as the initial value to save iteration time.

The adequacy of the method has been confirmed by comparing numerical solutions with analytical and experimental ones in a coaxial cylindrical field.[14]

The single pin-to-plate electrode is simplified to the two-dimensional coaxial cylindrical system and numerical calculations have been conducted using the finite element method. Figure 3 shows a mesh pattern of the finite element calculation. Instead of the infinite boundaries, large distances from the tip of the pin (r = 60 mm, z = 60 mm) are determined as the insulative boundary. The tip of the pin electrode is assumed semispherical and the domain in the vicinity of the tip was finely meshed. The mobility of the positive discharge ω_+ used for calculation is equal to that of positive ions in air, 1.9 $\times$ 10^{-4} m^2/Vs, whereas that of the negative discharge ω_- is assumed to be 10×10^{-4} m^2/Vs that is four times larger than that of negative ions in air. The adequacy of adapting this value is discussed in the later section.

Although it is reported that the preferred relaxation coefficient K is 0.52 for the rapid iteration in the coaxial cylindrical system,[14] it is set to be 0.4 in this calculation to avoid the risk against numerical divergence during the iteration calculation. Number of iteration steps was several hundred and the calculation time was about 3 hours for a fixed geometry and about fifteen steps of voltage using a popular DOS/V PC (Pentium III, 500 MHz).

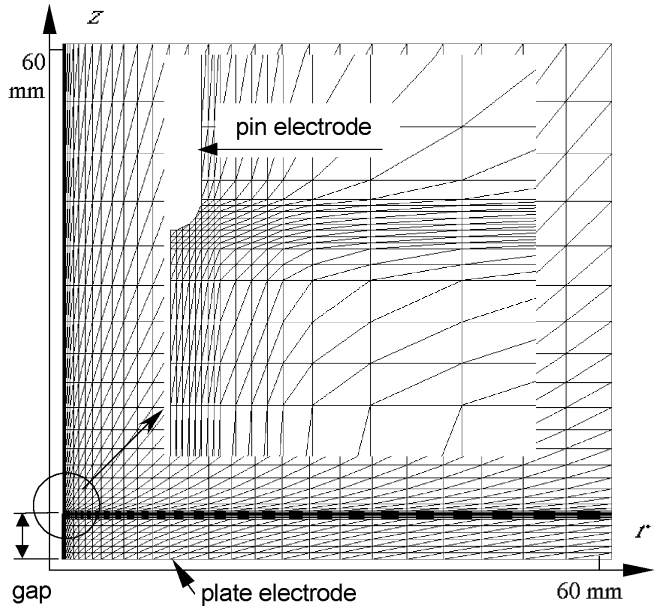

Figure 3. Linear triangular mesh pattern for FEM calculation. (number of nodal points = 1480, number of element = 2805).

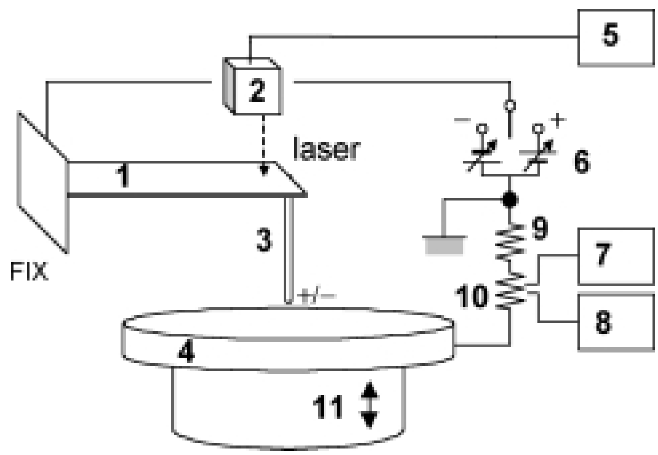

Figure 4. Experimental set-up. (1: stainless steel plate, cantilever, (1) low stiffness T0.1/L140/W10 mm, (2) high stiffness T0.1/L100/W20 mm; 2: laser sensor; 3: pin electrode, SUS304, ϕ 0.2, ϕ 0.3, ϕ 0.4, ϕ 0.5 mm; 4: plate electrode, steel; 5: laser displacement meter; 6: DC high voltage power supply; 7: DC volt meter; 8: oscilloscope; 9: resistor, 500 kΩ; 10: shunt resistor, 100 kΩ; 11: mechanical stage).

Experimental

Figure 4 shows an experimental set-up. A wire made of stainless steel was hung down perpendicular to a steel plate. The diameters of the wire used for experiment were 0.2, 0.3, 0.4, and 0.5 mm. It was connected to the free end of the cantilever plate made of stainless steel. The displacement at the free end of the cantilever was measured by a laser displacement meter (Keyence Corp., Tokyo, LK-2000) and the electrostatic

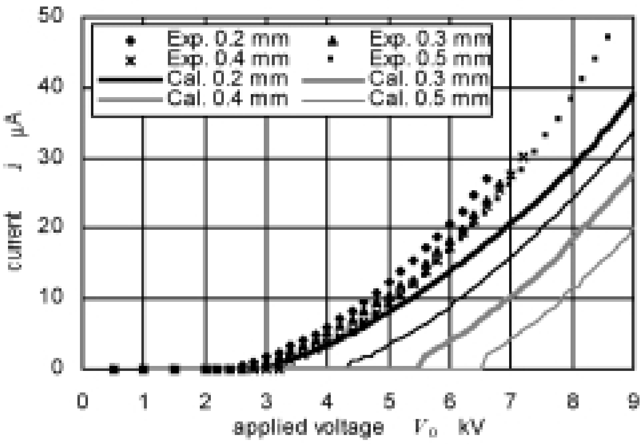

Figure 5. V-I curve in pin-to-plate electrode system. (positive charge, pin diameter: parameter, 5 mm air gap).

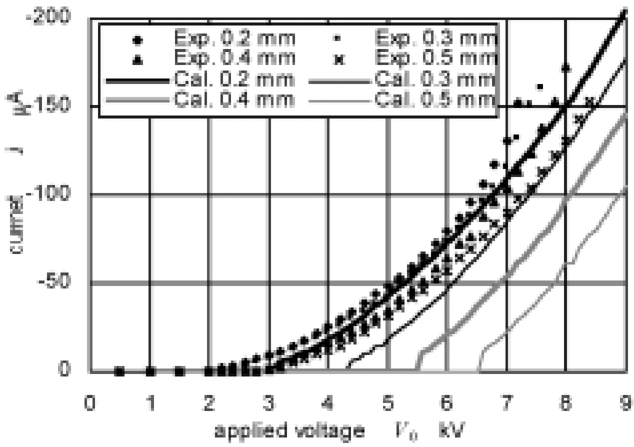

Figure 7. V-I curve in pin-to-plate electrode system. (negative, pin diameter: parameter, 5 mm air gap).

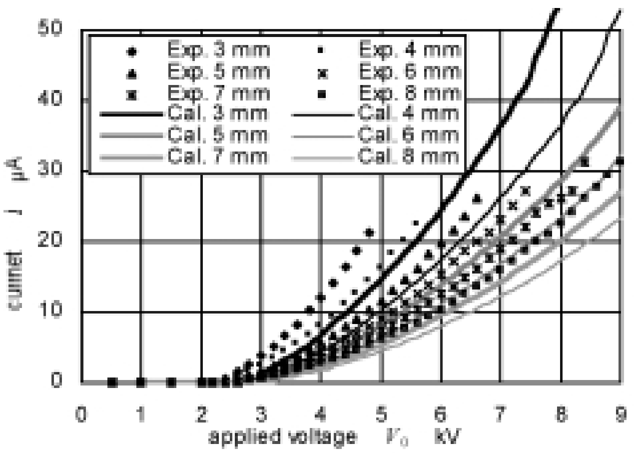

Figure 6. V-I curve in pin-to-plate electrode system. (positive, ϕ 0.2 mm pin diameter, air gap: parameter).

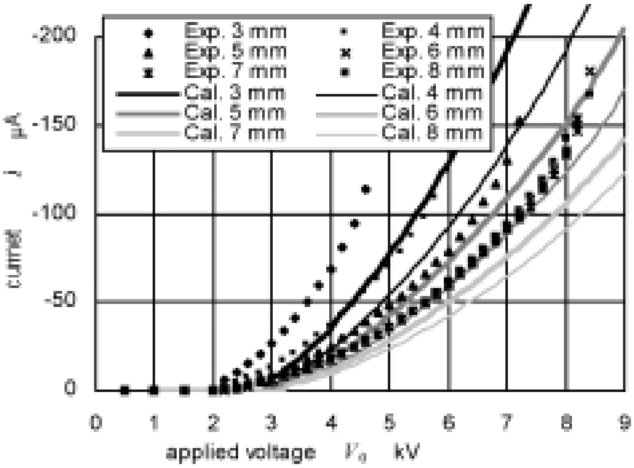

Figure 8. V-I curve in pin-to-plate electrode system. (negative, ϕ 0.2 mm pin diameter, air gap: parameter).

force to the pin was derived multiplying the measured displacement and the stiffness of the cantilever. Two plates were prepared; low stiffness (0.000377 N/mm) and relatively high stiffness (0.00231 N/mm). The former was used to measure extremely low force observed at low applied voltage and the latter was for the measurement of relatively large force at corona discharge. The stiffness was statically measured dividing weights put on the free end of the plate by the static displacement measured by the laser displacement meter. Because the electrostatic force to the wire was less than 400 μN and thus the axial displacement of the pin was less than 0.17 mm, change of the gap during discharging was negligible compared with the air gap, larger than 3.0 mm. It was also confirmed that the force measured with a half-length plate coincided with that with the regular plate. Gap between the wire and the plate was adjusted using a mechanical stage attached at the back of the plate electrode. High voltage was applied to the gap by a DC power supply (Matsusada Precision Inc., Tokyo, HVR-10P (positive) and HVR-10N (negative), 0 ~ ± 10 kV adjustable, maximum current 0.15 mA). Voltage was determined by a calibrated potentiometer of the power supply and current was measured by the voltage drop in a current-shunt resistor. The surface of electrodes was frequently polished to prevent oxidation and chemical deposition on the tip of the discharge electrode due to gas discharge. Reproducibility of data was confirmed during experiments.

Results and Discussion

Voltage-Current Characteristics

Figures 5 through 8 show measured and calculated voltage-current characteristics. Parameters are; positive or negative charge, the pin diameter, and the air gap. In many cases, fundamental features were similar with those of the corotron. At voltage lower than the threshold (2–3 kV), no substantial current flowed in the air gap. However, over the threshold voltage, the discharge current in the order of several microamperes was measured and at the same time weak luminescence was observed at the tip of the pin electrode. That is, corona discharge took place. The current and luminescence were stable and the discharge was silent. If the applied voltage was increased, the corona discharge shifted to the spark discharge. (Maximum values of applied volt-

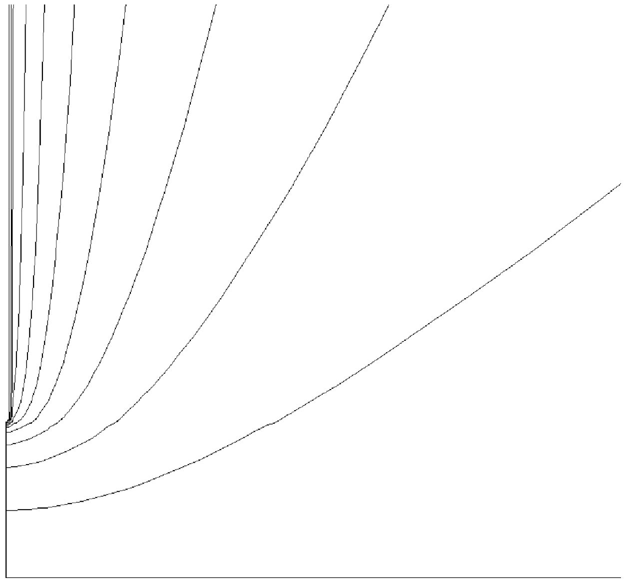

Figure 9. Potential distribution without discharge. (ϕ 0.2 mm pin diameter, 5 mm gap).

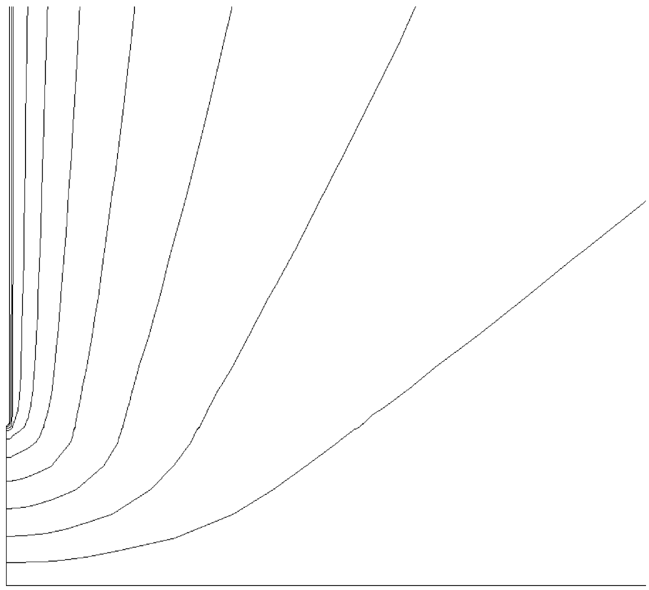

Figure 10. Potential distribution under discharge. (positive, ϕ 0.2 mm pin diameter, 5 mm air gap, V_0 = 4 kV).

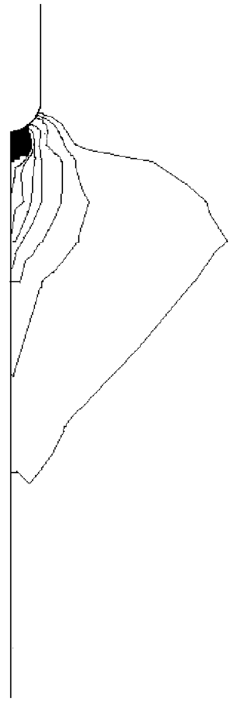

Figure 11. Distribution of charge density in the vicinity of the tip of the pin electrode under discharge. (positive, ϕ 0.2 mm pin diameter, 5 mm air gap, V_0 = 4 kV).

age plotted in the figures were thresholds of the spark discharge.) Because the spark discharge is non-self-sustaining, the discharge was not continuous but intermittent. When the mode of discharge just changed from the corona to the spark, vertical vibration of the pin electrode took place. Details of this interesting phenomenon will be reported in a separate study. Because the current was restricted by the capacity of the power supply, the arc discharge did not take place.

The calculated result qualitatively agreed with the measured. At the voltage lower than the threshold, although very low current is calculated depending on the initial value of the charge density, it is negligibly small (in the order of 10^{-12} A). However, when the voltage is further increased and the electric field on the discharge electrode reaches the threshold, current begins to flow because the charge density at the corresponding part becomes large to suppress the increase of the electric field. Thus, the electric field at the tip of the pin electrode is maintained at the threshold. This is the reason for the experimental evidence that the corona onset voltage was low and the corona current was high with small pin diameter and small air gap. It is recognizable by observing the distributions of the potential and the charge density. Figure 9 shows the potential distribution without discharge and Fig. 10 is that under discharge. Curved lines indicate the equipotential surfaces designating 10 per cent of the total applied voltage V_0. Figure 11 is the distribution of the charge density in the vicinity of the tip of the pin electrode under discharge. The calculation condition of Fig. 11 is common with that of Fig. 10. It is clearly understood from these figures that when high voltage is applied, the air is ionized and charge is yielded in the vicinity of the tip[15] where the electric field reaches the threshold of the corona onset. Careful comparison of Fig. 9 and Fig. 10 leads us to recognize that the generation of charge at the tip results in the relaxation of the electric field. The discharge region becomes wide under high voltage application. This corresponds to the experimental observation that luminescence becomes strong under high voltage.

The following characteristics are recognized from Figs. 5 through 8 on the effects of the pin diameter, the air gap, and positive or negative discharge.

(1) The corona onset voltage was low and the corona current was high with small pin diameter and small air gap both in positive and negative corona. However, measured results did not qualitatively agree with

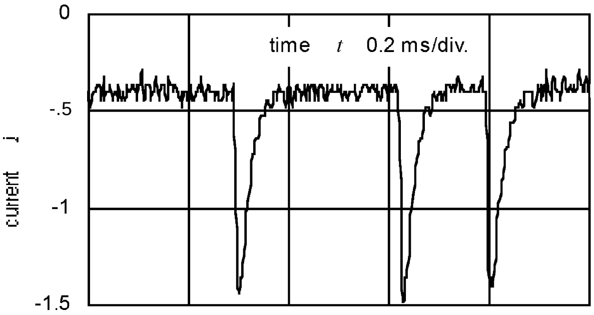

Figure 12. Trichel pulse. (negative, ϕ 0.2 mm pin diameter, 5 mm air gap, V_0 = 3 kV) Vibration of the pin electrode caused fluctuation of pulse frequency. Corona current was measured by the oscilloscope to eliminate Trichel pulse when it took place at the beginning of the negative corona discharge.

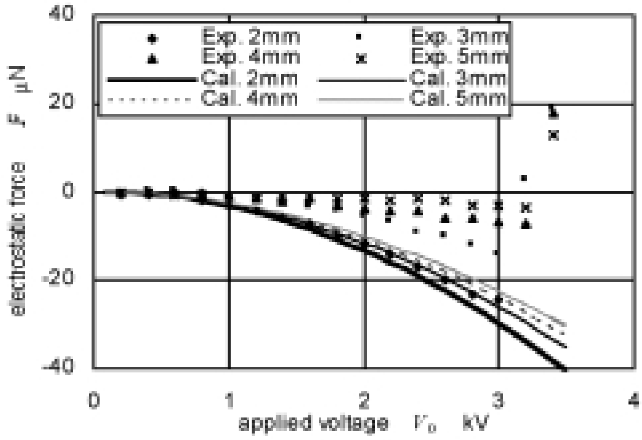

Figure 13. Electrostatic force applied to pin electrode at low voltage. (positive, 0.5 mm pin diameter, air gap: parameter).

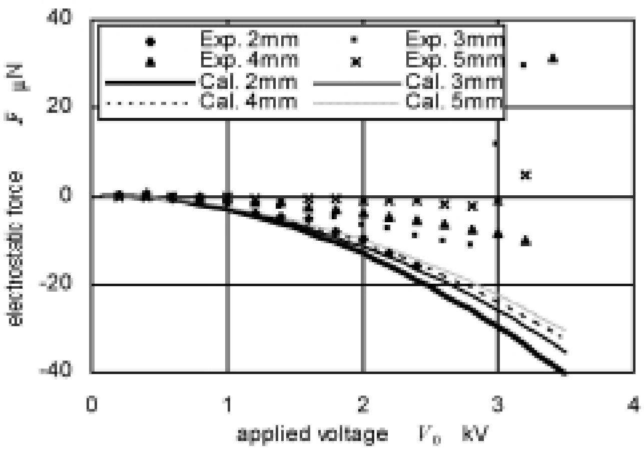

Figure 14. Electrostatic force applied to pin electrode at low voltage. (negative, 0.5 mm pin diameter, air gap: parameter).

the calculated that the corona onset voltage and current were highly dependent of the pin diameter. This is probably because the pin tip used for experiment was not exactly semi-spherical but somewhat sharp. Details are discussed in the later section on the effect of sharpness of the pin electrode.

(2) The onset voltage of the negative corona was almost the same with that of the positive corona but the current was about four times larger than the positive. A similar characteristic was reported in Ref. 16. A possible reason of the discrepancy is due to the difference of the charged particles that contribute to electric conduction. Although the conduction in the positive discharge is solely due to positive ions, not only negative ions but also electrons contribute to the electric conduction in the negative corona. In case of an electron beam printhead, it is reported that the charge deposited in a dielectric film is predominantly electrons.[13,17] Experimental results indicate that about 80% of the total charge is due to electrons.[17] This is not exactly the case of the present system whose air gap is larger than that of the electron beam printhead, 250 μm. Nevertheless the current may be high even though the rate of electrons is small because the mobility of electron is about 400 times larger than that of the negative ion. Although the effective mobility of the negative discharge is not clear, the measured V-I characteristics agreed fairly well with the calculated if the negative mobility is assumed to be 10×10^{-4} m^2/Vs, that is, four times larger than that of negative ions in air. A multi-component model must be established to confirm the hypothesis.

(3) Trichel pulse[18] takes place at relatively low applied voltage in the pin-to-plate negative corona discharge system as shown in Fig. 12. The occurrence of Trichel pulse is one of major differences of the pin-to-plate system to the wire-to-plate or coaxial cylindrical systems. A time-dependent model must be established to clarify this unique phenomenon.

Electrostatic Force

Figures 13 and 14 are the measured and calculated electrostatic force to the pin electrode under low applied voltage in the positive and negative discharge, respectively. Measurement was done using the low stiffness cantilever. The force acts in the vertical direction and the repulsive force applied in the upward direction is designated as positive. Even at the voltage lower than the threshold, a small force was induced. It was only in the order of 10 μN. The force is proportional to a square of the voltage and independent of positive or negative. The calculated result was similar to the measured one. However, although the dependence of the air gap was small in the calculation, it was large in the measured. Possible reasons for this disagreement are the non-spherical configuration of the pin tip and the poor reliability of data at extremely low force.

Over the threshold voltage, the force was *repulsive* and became large, in the order of 100 μN, in accordance with the increase of voltage as shown in Figs. 15 through 18. It showed little dependence to the air gap, the pin diameter, and the difference of positive or negative corona. On the other hand, the calculated force is applied downward and almost constant with respect to the voltage. This is because it is assumed in the model that the electrostatic field is maintained constant at the surface of the pin electrode during corona discharging and only the discharge area becomes larger with the increase of voltage. A similar characteristic was reported in the wire-to-plate system.[11] However, in the present pin-to-plate system, the calculation was completely different to the measured system. Preliminary experiments to visualize

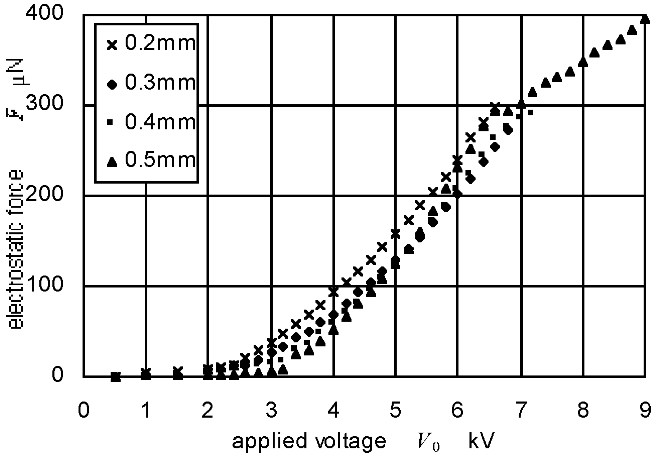

Figure 15. Electrostatic force applied to pin electrode at corona discharge. (positive, pin diameter: parameter, 5 mm air gap).

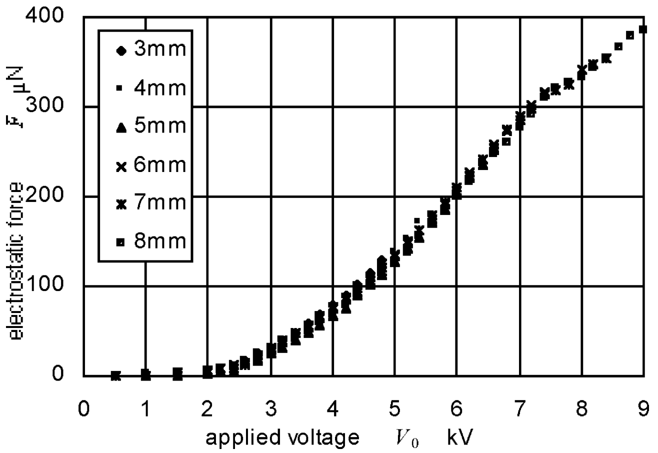

Figure 16. Electrostatic force applied to pin electrode at corona discharge. (positive, ϕ 0.2 mm pin diameter, air gap: parameter).

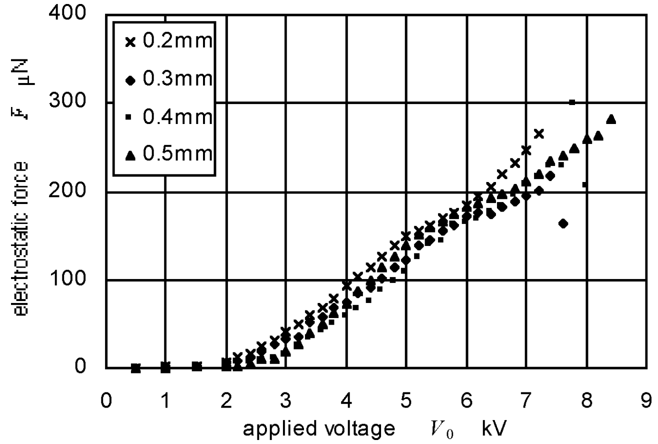

Figure 17. Electrostatic force applied to pin electrode at corona discharge. (negative, pin diameter: parameter, 5 mm air gap).

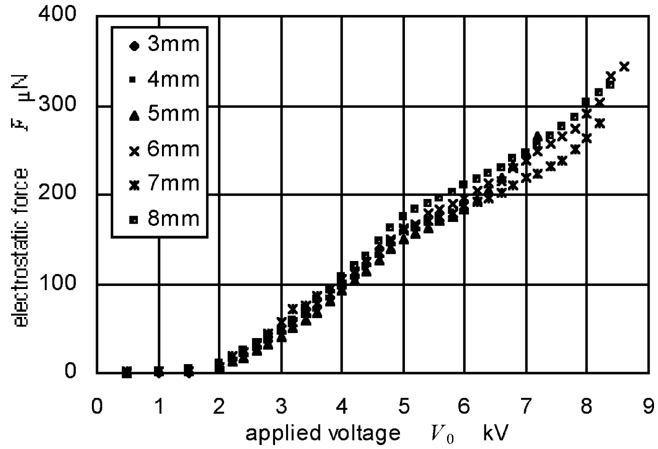

Figure 18. Electrostatic force applied to pin electrode at corona discharge. (negative, ϕ 0.2 mm pin diameter, air gap: parameter).

airflow in the vicinity of the pin electrode suggested that the convection of the air, ionic wind, which is neglected in the model, performed an important role in the kinetics of the electrode. The present simulation model must be refined to include not only time dependency and multi-component features, but also diffusion and convection of gases. Although the force was very small compared with that in the wire-to-plate system, it is large enough to change the form of the brush or magnetic bead chains and it is large by more than two orders of magnitude, compared with the magnetic force to carrier beads in the magnetic development subsystem (in the order of 0.1 ~ 1 µN). The electrostatic force is one of the most important factors that affect the bead carry-out.

Effect of Sharpness of Pin Electrode

Although the tip of the pin electrode was assumed to be semispherical in the numerical calculation, it was in reality somewhat sharp. The effect of the sharpness was experimentally investigated using spherical and sharpened electrodes as shown in Fig. 19. It was clarified that the corona onset voltage was highly dependent on the shape of the pin tip as shown in Fig. 20. If a sharp edge existed at the pin tip, the corona discharge took place at low voltage because the corona onset electric field was high at the sharp edge even when the pin diameter was large. On the other hand, electrostatic force, both at low voltage less than corona onset and at corona discharging, was not affected by the sharpness of the pin electrode as shown in Figs. 21 and 22. This corresponded to the experimental results that the force showed small dependence on the diameter of the pin electrode.

Effect of Tilting of Pin Electrode

It is impossible in an actual machine to set the pin electrode exactly at a right angle to the plate electrode, particularly in the case when a brush or magnetic bead chains are used for pin electrodes. Carrier chains in the two-component magnetic brush development subsystem are also not at right angles to the photoconductor but chains align along the magnetic flux line.[2] Because the system is not symmetrical when the pin electrode is not perpendicular to the plate, numerical calculations could not conducted but the effect of tilting of the pin electrode was experimentally investigated. The result is shown in Figs. 23 and 24. It is clearly recognized from these figures that the effect of tilting is negligible with respect to both the current and the force even when the

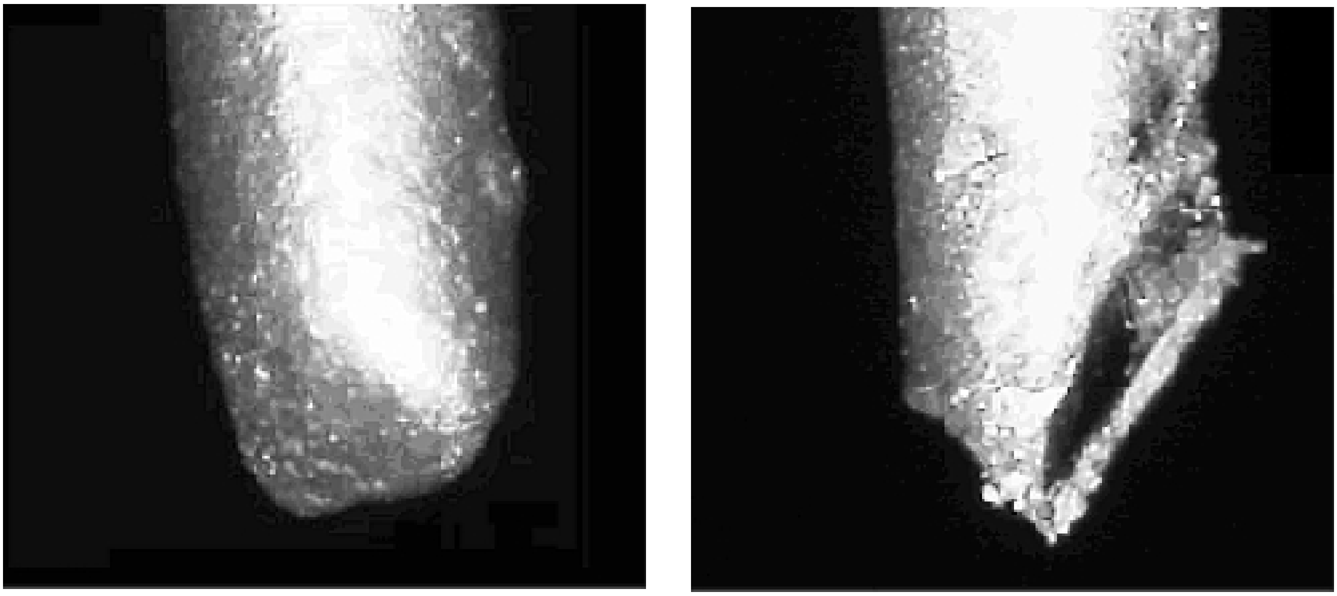

(a) spherical (b) sharpened

Figure 19. Tip of pin electrode.

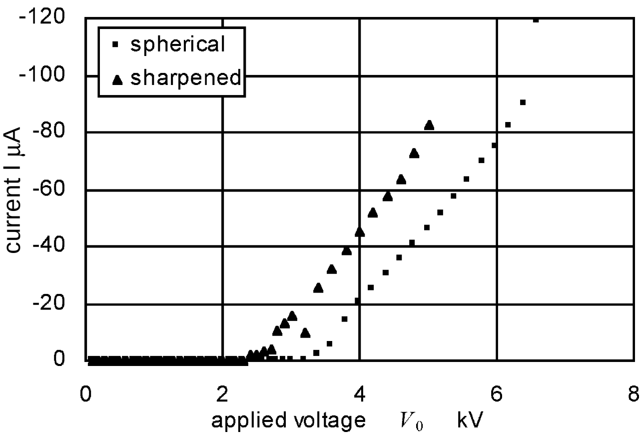

Figure 20. V-I curves with spherical and sharpened pin electrodes. (negative, ϕ 0.5 mm pin diameter 3 mm air gap).

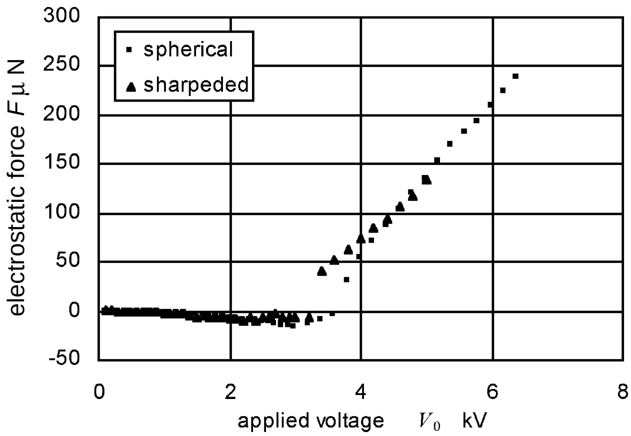

Figure 22. Electrostatic force applied to spherical and sharpened pin electrodes at corona discharge. (negative, ϕ 0.5 mm pin diameter, 3 mm air gap).

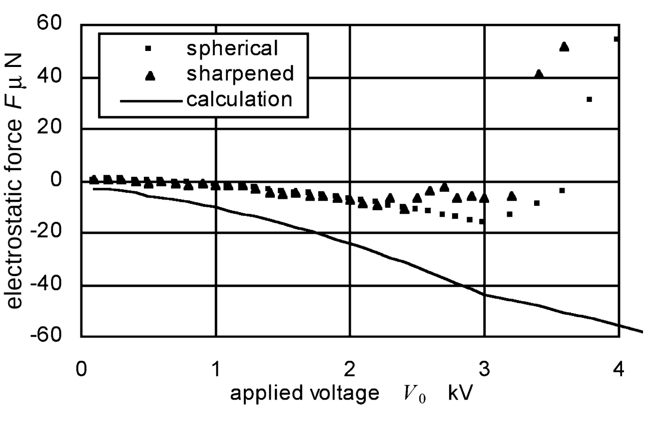

Figure 21. Electrostatic force applied to spherical and sharpened pin electrodes at low voltage. (negative, ϕ 0.5 mm pin diameter, 3 mm air gap).

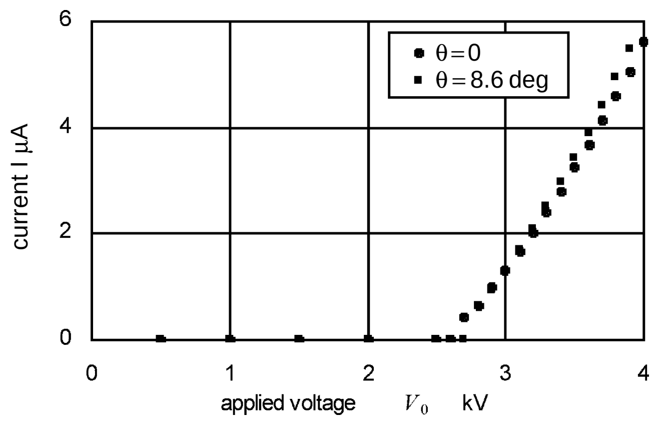

Figure 23. V-I curve in pin-to-plate system in case that the electrodes are not exactly in right angle. (positive, ϕ 0.2 mm pin diameter, 5 mm air gap).

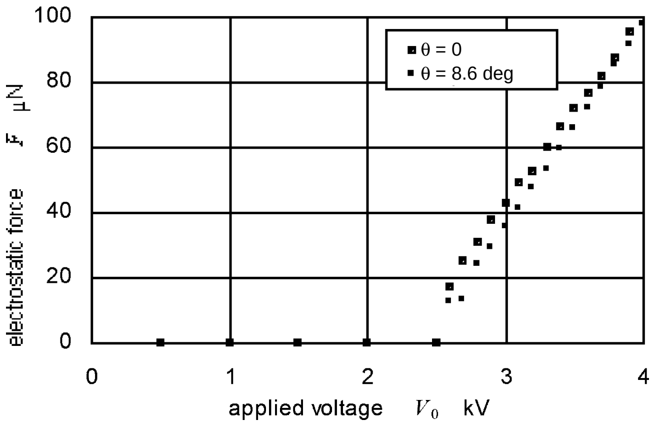

Figure 24. Electrostatic force applied to pin electrode in case that the electrodes are not exactly in right angle. (positive, ϕ 0.2 mm pin diameter, 5 mm gap).

tilt was substantial. This is probably because both the current and the force are determined at the tip of the pin electrode, and the contribution of the other surface is small.

Concluding Remarks

Statics of the pin electrode in the pin-to-plate system has been investigated to utilize the system for a new low ozone charger and to clarify the fundamental mechanism of bead carry-out in the two-component magnetic brush development subsystem of electrophotography. The following is a summary of the investigation.

Voltage-Current Characteristics

The corona discharge took place above a threshold voltage. The corona onset voltage is low and the corona current is high for small pin diameters and small air gap both in positive and negative corona. The onset voltage of the negative corona was almost the same as that of the positive corona, but the measured current was about four times larger than the positive. Numerical calculation was conducted to calculate the corona current and the electrostatic force. The model is static and unipolar and it neglects the effects of diffusion and convection of charged particles. It is assumed that generation of ions takes place on a tip of the pin electrode and that surface electric field is less than the onset field of corona discharge. Calculated voltage-current characteristics qualitatively agreed with the measured, but a dynamic and multi-component model is necessary to clarify the quantitative characteristics including Trichel pulse observed at the start of the negative corona.

Electrostatic Force

Although extremely small electrostatic pull force, in the order of 10 μN, was induced if discharge did not take place, the force became repulsive and relatively large, in the order of 100 μN when the corona discharge took place. Calculated force without discharge agreed with the measured, but the calculation did not simulate repulsive characteristics at corona discharging. Preliminary experiments to visualize airflow in the vicinity of the pin electrode suggested that the convection of the air, ionic wind, must be included in the model.

Effect of Sharpness

If a sharp edge existed at the pin tip, the corona discharge took place at low voltage because the corona onset electric field was high at the sharp edge even when the pin diameter was large. On the other hand, electrostatic force was not affected by the sharpness of the pin.

Effect of Tilting

The effect of tilting of the pin electrode is negligible even when the tilt is substantially large (8°) probably because both the current and the force are determined almost at the tip of the pin electrode and contribution of the other surfaces is small.

Acknowledgment. The author would like to express his thanks to Kosuke Takasaki, Hiromu Yasuda, and Naohiro Kumagai for their help of carrying out experiments. This work is supported by The Iwatani Naoji Foundation's Research Grant.

References

1. T. B. Hansen and B. Andersen, *Am. Ind. Hyg. Assoc. J.* **47**, 659 (1986).
2. E. M. Williams, *The Physics and Technology of Xerographic Processes*, Krieger Publishing Co., Malabar, FL, 1992.
3. H. Kawamoto, *J. Imaging Sci. Technol*, **39**, 439 (1995).
4. J. Araya, N. Koitabashi, S. Nakamura and H. Hirabayashi, US Patent 5,164,779 (1992).
5. J. Araya, N. Koitabashi, S. Nakamura and H. Hirabayashi, Eur. Patent 280 542 (1988).
6. H. Kawamoto and H. Satoh, *J. Imaging Sci. Technol.* **38**, 383 (1994).
7. H. Kawamoto, *J. Imaging Sci. Technol.* **39**, 267 (1995).
8. K. Furukawa, H. Ishii, K. Shiojima and T. Ishikawa, *IS&T's Tenth International Congress on Advances in Non-Impact Printing Technologies*, IS&T, Springfield, VA, 1994, p. 34.
9. K. Furukawa, H. Ishii, K. Shiojima and T. Ishikawa, *Electrophoto.* **35**, 116 (1996).
10. H. Kawamoto, *J. Imaging Sci. Technol.* **44**, 452 (2000).
11. Y. Ito, Dynamics of the Wire Electrode in a System of Wire and Plate Electrodes, Ph.D. Thesis, Keio University, 1996.
12. M. Farzaneh and Y. Teisseyre, *IEEE Trans. on Power Delivery*, **3**, 1122 (1988).
13. H. Kawamoto and S. Serizawa, *J. Imaging Sci. Technol.* **41**, 629-632 (1997).
14. M. Hattori and K. Asano, *Trans. IEE Japan*, **106A**, 95 (1986).
15. P. J. Walsh, K. W. Pietrowski and R. S. Sigmond, *Photographic Sci. Eng.* **28**, 101 (1984).
16. W. L. Lama and C. F. Gallo, *IEEE Trans. Industry Application*, IA-12, 288 (1976).
17. W. J. Caley, W. R. Buchan and T. W. Pape, *J. Imaging Sci. Technol.* **17**, 51 (1991).
18. W. L. Lama and C. F. Gallo, *J. Appl. Phys.* **45**, 103 (1974).